symmetry

MDPI

Article

New High-Pressure Structures of Transition Metal Carbonates with $O_3C–CO_3$ Orthooxalate Groups

Nursultan E. Sagatov [1,2,*], Dinara N. Sagatova [1,2], Pavel N. Gavryushkin [1,2] and Konstantin D. Litasov [3,4]

1 Sobolev Institute of Geology and Mineralogy, Siberian Branch of Russian Academy of Sciences, 630090 Novosibirsk, Russia
2 Novosibirsk State University, Department of Geology and Geophysics, 630090 Novosibirsk, Russia
3 Vereshchagin Institute for High Pressure Physics, Russian Academy of Sciences, Troitsk, 108840 Moscow, Russia
4 Fersman Mineralogical Museum, Russian Academy of Sciences, 119071 Moscow, Russia
* Correspondence: sagatinho23@gmail.com or sagatovnye@igm.nsc.ru; Tel.: +7-952-940-3247

Abstract: Based on the density functional theory and crystal structure prediction approaches, we found a novel high-pressure structure of Fe_2CO_4-$P\bar{1}$. It is characterized by the presence of ethane-like $O_3C–CO_3$ groups or so-called orthooxalate groups. The formation of such $O_3C–CO_3$ groups has been proposed earlier in melts and aqueous carbonate solutions, but no such examples were known in inorganic crystalline materials. We found that this structure is dynamically and thermally stable at pressures of 50 GPa. Similar structures were also predicted to be dynamically stable for Mn_2CO_4, Ni_2CO_4, and Co_2CO_4. In addition, $FeCO_3$ was found to transform into a similar structure with $O_3C–CO_3$ orthooxalate groups at a pressure above 275 GPa. Additionally, for the first time, we describe the self-diffusion of metal atoms in carbonates at high pressure and at high temperatures. The prediction of novel carbonate structures extends the crystal chemistry of inorganic carbonates beyond the established ones with $[CO_3]$ triangles, $[C_2O_5]$ pyro-groups, and $[CO_4]$ tetrahedra.

Keywords: orthocarbonates; high pressure; crystal structure prediction; density functional theory; siderite

Citation: Sagatov, N.E.; Sagatova, D.N.; Gavryushkin, P.N.; Litasov, K.D. New High-Pressure Structures of Transition Metal Carbonates with $O_3C–CO_3$ Orthooxalate Groups. *Symmetry* **2023**, *15*, 421. https://doi.org/10.3390/sym15020421

Academic Editors: Alexey V. Lukoyanov and Sergei D. Odintsov

Received: 31 December 2022
Revised: 31 January 2023
Accepted: 1 February 2023
Published: 5 February 2023

1. Introduction

Currently, theoretical methods for crystal structure predictions have proven to be an effective approach for discovering new compounds and their structures that precede real experiments. Recently, using these methods, it was shown that in the MO–CO_2 systems (where M = Mg, Ca, Sr, Ba, and Pb), in addition to the well-known MCO_3 carbonates, M_2CO_4, M_3CO_5, and MC_2O_5 compounds became thermodynamically stable at high pressures [1–5]. Subsequently, the formation of the Mg_2CO_4 [6], Ca_2CO_4 [7], CaC_2O_5 [8], Sr_2CO_4 [9], Sr_3CO_5 [10], SrC_2O_5 [11], and PbC_2O_5 [12] phases was experimentally confirmed.

For alkaline earth metals, the thermodynamic stabilization pressures of M_2CO_4 structures (M = Mg, Ca, Sr, and Ba) were inversely proportional to the cation size, decreasing from 50–75 GPa for Mg^{2+} [3,6] to 5 GPa for Ba^{2+} [4]. Ca_2CO_4, Sr_2CO_4, and Ba_2CO_4 have the same structure *Pnma*, while Mg_2CO_4 has slightly different structure ($P2_1/c$) [6]. The low-pressure thermodynamic stability limits for the crystal structures of M_3CO_5 (M = Ca, Sr, and Ba) compounds vary in the range of 11–15 GPa, and these compounds are stable in the $I4/mcm$ structure [4].

The structures of M_2CO_4 and M_3CO_5 are characterized by the presence of orthoanion groups of $[CO_4]$ tetrahedra and form a class of orthocarbonates and oxy-orthocarbonates. The sp^3-hybridized carbon atoms in the structures of orthocarbonates are a key difference from the so-called "traditional" MCO_3 carbonates, whose structures contain sp^2-hybridized carbon atoms only in triangular coordination at a pressure below 50 GPa. The structures of the MC_2O_5 composition are characterized by the most diverse crystallochemistry, including

$[C_2O_5]$ pyro-groups (formed by two trigonal $[CO_3]$ groups), complex tetrahedra, layers, and frameworks which consist of corner-shared $[CO_4]$ tetrahedra [1,8,13]. In addition, at pressures above 70 GPa, traditional carbonates $MgCO_3$ and $CaCO_3$ are known to transform into structures that consist of corner-shared $[CO_4]$ tetrahedra, forming chains or rings [14–17].

For iron, in addition to the traditional carbonate $FeCO_3$, $Fe_4C_3O_{12}$ and $Fe_4C_4O_{13}$ are also known [18]. Both carbonates contain tetrahedrally coordinated carbon units and are formed above ~70 GPa [18]. However, these two carbonates contain iron in both 2+ and 3+ oxidation states and are beyond the FeO–CO_2 system. Hence, to date, $FeCO_3$ is the only known intermediate compound in this system. It should also be noted that, unlike $MgCO_3$ and $CaCO_3$, iron carbonate does not undergo polymorphic phase transitions up to 110 GPa [18–20].

The aim of the present work is to reveal the possible stable structure of Fe_2CO_4 and $FeCO_3$ using crystal structure prediction methods. The obtained results could extend the known crystal chemistry of inorganic carbonates and motivate future experimental studies of the FeO–CO_2 system, which is complicated by the presence of iron in two oxidation states.

2. Computational Methods

Crystal structure prediction has been performed using evolutionary algorithms implemented in the USPEX package [21–24] and random structure searching implemented in the AIRSS package [25,26] at 25, 50, 75, and 100 GPa for fixed-composition Fe_2CO_4 and at 100, 200, and 300 GPa for $FeCO_3$ for 1–4 formula units per unit cell.

The first generation in the USPEX calculations consisted of 65 structures created using a random symmetry operator. Furthermore, to obtain the next generation, 60% of the structures with the lowest enthalpy from the previous generation were selected. In all subsequent generations, structures were produced by heredity (35%), atomic mutation (20%), lattice permutation (10%), and random generator (35%) operators. On average, 32–36 generations were produced and relaxed at each pressure.

All calculations were performed within the VASP 5.4.4 package [27,28] based on density functional theory (DFT). The exchange-correlation effects were calculated via generalized gradient approximation (GGA) in Perdew–Burke–Ernzerhof (PBE) parameterization [29]. To describe core-valence interactions, we used the projector augmented wave basis set with energy cutoff of plane waves equal to 430 eV. The first Brillouin zone was sampled according to the Monkhorst–Pack scheme with a *k*-point mesh of 0.5 $Å^{-1}$ and Gaussian smearing with a parameter σ = 0.1 eV. The most promising predicted structures were relaxed with higher accuracy as follows: the cutoff energy was 600 eV, *k*-point sampling grid of spacing was 0.25 $Å^{-1}$, and σ = 0.05 eV. Pseudopotentials with $3d^7 4s^1$ (Fe), $2s^2 2p^2$ (C), and $2s^2 2p^4$ (O) electronic configurations were used.

It is well-known that standard DFT tends to over-delocalize the electronic states for transition metals, which prevents them from describing the systems with strongly localized *d*-electrons appropriately. In order to describe the properties of considered structures more accurately, Dudarev's DFT+U method was used [30]. In our study, U was set to 2 eV, since in [31], it was found to give the best agreement with the experimental values for the spin transition pressure of iron in $FeCO_3$.

Calculations of the phonon spectra were performed using the PHONOPY program [32]. The real space force constants were calculated using supercell and finite displacement approaches, with 2 × 2 × 2 supercells for the considered structures. In this case, high-quality settings were used: the cutoff energy was 800 eV, *k*-point sampling grid of spacing was 0.2 $Å^{-1}$, and σ = 0.05 eV.

To examine the thermal stability of Fe_2CO_4, ab initio molecular dynamic (AIMD) simulations based on DFT were performed using a supercell with 255 atoms at 300, 1000, and 2000 K. The time step was set to 1 fs. In the simulations at 300 and 1000 K, the total simulation time was 10 ps, and in the simulations at 2000 K, it was 20 ps. The *NPT* ensemble

(where N is the number of particles, P is pressure, and T is the temperature) were used. During the simulation, the frequency of the temperature oscillations was controlled by the Langevin thermostat.

Images of the structures were produced using VESTA software [33]. The MD simulation animation was made in OVITO software [34].

3. Results

Experiments performed for Fe_2CO_4 crystal structure predictions have revealed the known structures of Ca_2CO_4-*Pnma* [2] and Mg_2CO_4-*Pnma* (Olivine type) [3]. However, these structures are not the most favorable among the predicted ones. According to the results obtained, the structure with $P\bar{1}$ symmetry had the lowest enthalpy in the entire studied pressure range of 10–100 GPa (Figure 1a). The predicted Fe_2CO_4-$P\bar{1}$ was dynamically stable, as evidenced by the absence of imaginary frequencies in the calculated phonon spectrum (Figure 1b).

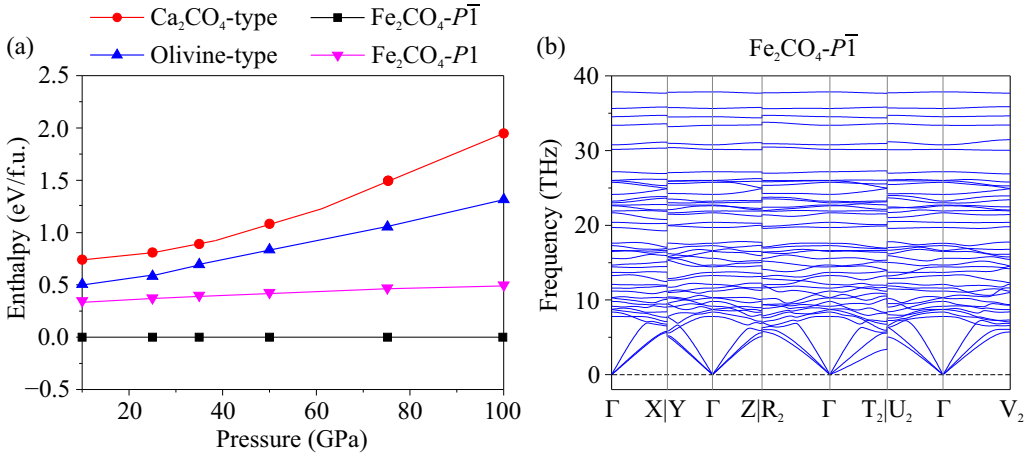

Figure 1. (**a**) Relative enthalpy-pressure dependencies of Fe_2CO_4 modifications. (**b**) Phonon dispersion curves of Fe_2CO_4-$P\bar{1}$ at 50 GPa.

In DFT+U calculations, the total energy of a phase strongly depends on the Hubbard correction U. Since U must vary for each compound, it makes no sense to compare the total energies obtained from the calculations with the same values of U, and it is incorrect to compare the energies obtained with different U values. Consequently, estimation of the pressure at which Fe_2CO_4-$P\bar{1}$ became stable relative to decomposition into carbonate and oxide is currently difficult. For instance, we estimated the stability of Fe_2CO_4-$P\bar{1}$ relative to FeO in the wustite structure and $FeCO_3$ in the siderite structure without consideration of Hubbard correction (U = 0) and with U = 2 eV (Figure 2), respectively. In the first case, Fe_2CO_4-$P\bar{1}$ stabilizes with respect to a mechanical mixture of FeO + $FeCO_3$ above 40 GPa. In the second case, it stabilizes at sufficiently higher pressures above 100 GPa. Thus, the stability of Fe_2CO_4-$P\bar{1}$ relative to FeO + $FeCO_3$ remains an open question.

The structural data of the predicted Fe_2CO_4-$P\bar{1}$ are given in Table 1. The structure was characterized by the presence of ethane-like [C_2O_6] groups, in which two carbon atoms were bonded together and, in addition, each of them bonded to three more oxygen atoms (Figure S1). By analogy with orthocarbonates, we will call such a group an *orthooxalate group* and label it as O_3C–CO_3. The found Fe_2CO_4-$P\bar{1}$ is the first example of inorganic compounds with the O_3C–CO_3 group. However, there exists one example of an organic compound with an orthooxalate group, namely a unique orthooxalate: 2,5,7,10,11,14-hexaoxa[4.4.4]propellane [35].

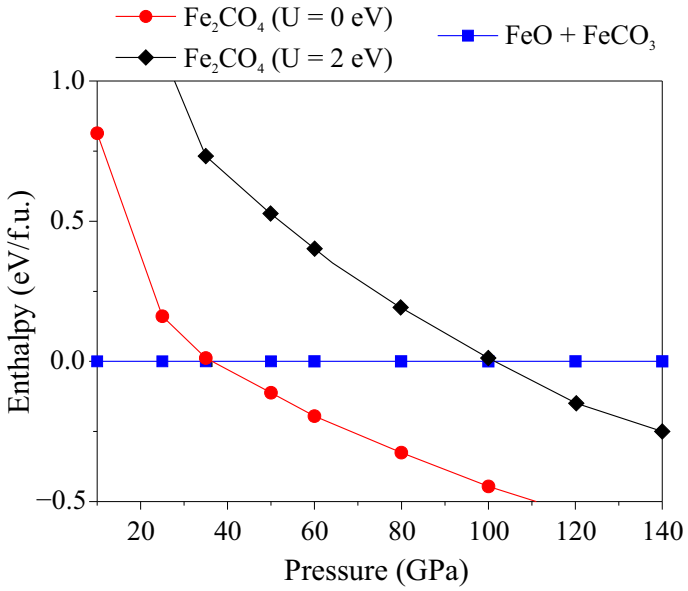

Figure 2. The enthalpy-pressure dependency of Fe_2CO_4-$P\bar{1}$ relative to the mechanical mixture of FeO + $FeCO_3$.

At 50 GPa, the C–C distances between two neighboring carbon atoms were equal to 1.53 Å, and the C–O distances varied in the range of 1.35–1.40 Å. These distances were almost equal to the bond lengths observed for the mentioned organic orthooxalate [35], in which the C–C bond length was 1.55 Å and the C–C bond was 1.395 Å. As expected, in the crystal structure of siderite $FeCO_3$-$R\bar{3}c$, the C–O distances were shorter, and they were equal to 1.27 Å at 50 GPa.

Similar to siderite, the crystal structure of Fe_2CO_4-$P\bar{1}$ can be described as the filling of octahedral voids by cations in the close packing of anions. The array of oxygen atoms in it corresponds to a slightly distorted *hcp* structure. Half of the octahedral voids are filled with Fe atoms, with 1/8 of them being filled with covalently bonded carbon atoms which are part of orthooxalate groups. In the structure, slabs A and B of the partially filled close-packed octahedra of oxygen atoms can be distinguished (Figure 3a). In slab A, half of the octahedra were filled with Fe atoms. The FeO_6 octahedra were connected in chains as shown in Figure 3b. In slab B, half of the octahedra were filled with Fe atoms, and one-fourth of the octahedra were filled with C–C groups (Figure 3c). Slabs A' and B' were similar to A and B in atomic arrangement but shifted in one octahedron, which could also be distinguished.

The atomic environment around the iron atoms had some similarities with the well-known ferrioxalate anion $[Fe(C_2O_4)_3]^{3-}$ [36] present in the tri-hydrated potassium tris(oxalato) ferrate(III) $K_3[Fe(C_2O_4)_3]\cdot 3H_2O$. Similar to this transition metal complex, in the found Fe_2CO_4-$P\bar{1}$ structure, iron was in octahedral coordination with an Fe–O distance nearly equal to 2 Å. The ferrioxalate anion consisted of an $[FeO_6]$ octahedron and three $[C_2O_4]^{2-}$ oxalate groups acting as bidentate ligands, while in the found Fe_2CO_4 structure, there was an $[FeO_6]$ octahedron and two bidentate orthooxalate $[C_2O_6]$ groups.

It should be noted that the second low-enthalpy phase Fe_2CO_4-*P*1 also had O_3C–CO_3 orthooxalate groups in its structure (Figure 1). Fe_2CO_4-*P*1 and Fe_2CO_4-$P\bar{1}$ were similar in the manner that they represented different fillings of octahedral voids in the *hcp* array of oxygen with Fe atoms and C–C groups (Table S1 and Figure S2).

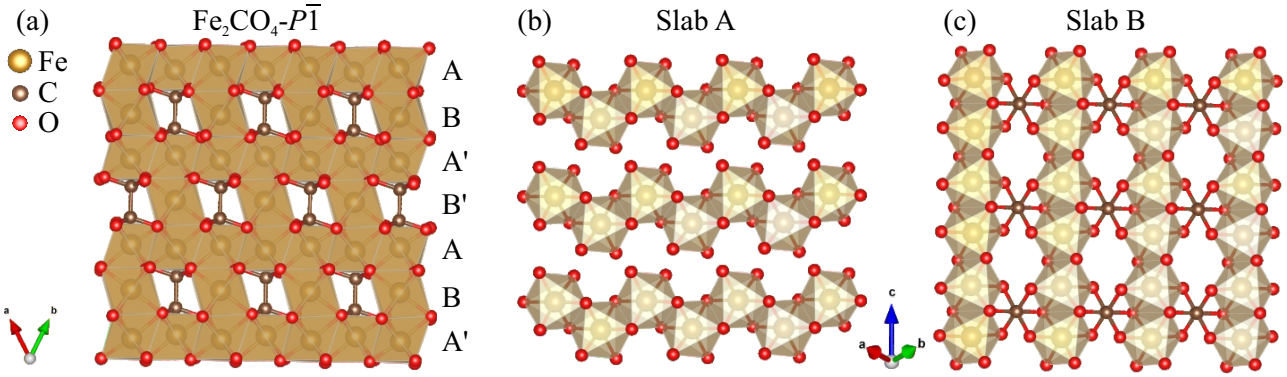

Figure 3. Crystal structure of predicted Fe_2CO_4-$P\bar{1}$.

Table 1. Structural data of predicted Fe_2CO_4 and $FeCO_3$ modifications with the lowest enthalpy.

Phase (#s.g.)	*P* (GPa)	Lattice Parameters (Å, deg)			Atom	Coordinates		
						x	y	z
Fe_2CO_4-$P\bar{1}$ (#2)	50	$a = 4.411$ $\alpha = 103.63$	$b = 5.038$ $\beta = 115.32$	$c = 5.112$ $\gamma = 90.81$	Fe	0.7775	0.3775	0.0286
					Fe	0.4953	0.2401	0.4757
					C	−0.0905	−0.0435	0.3287
					O	0.2903	0.2940	0.7483
					O	0.2825	0.8464	0.7596
					O	0.2239	0.4483	0.2571
					O	0.8404	0.0695	0.7651
$FeCO_3$-$P\bar{1}$ (#2)	250	$a = 3.910$ $\alpha = 91.75$	$b = 4.048$ $\beta = 116.73$	$c = 4.157$ $\gamma = 118.79$	Fe	0.6729	0.8428	0.4959
					C	0.8665	0.4328	0.2999
					O	0.5147	0.6023	0.7874
					O	0.8863	0.2857	0.7919
					O	0.1883	−0.0950	0.8004

In order to analyze the bonding nature, we calculated the Bader charges, the charge density differences (crystal density minus superposition of isolated atomic densities), and electron localization functions (ELFs) of Fe_2CO_4-$P\bar{1}$ at 50 GPa. The obtained Bader charge of C^{4+} in Fe_2CO_4-$P\bar{1}$ was lower than that of C^{4+} in $FeCO_3$-$R\bar{3}c$, being +1.609 and +2.109 for C^{4+} in Fe_2CO_4-$P\bar{1}$ and in $FeCO_3$-$R\bar{3}c$, respectively. This indicates that part of the electrons which were used for the formation of C–O bonds within the [CO_3] triangle was spent on the formation of a C – C bond. The calculated Bader charges of other atoms are summarized in Table 2. As shown in Figure 4, the charge accumulation occurred halfway through the C–C and C–O vectors. The maximum ELF value between two carbon atoms was about 0.9, and between the carbon and oxygen atoms, it was about 0.7 (Figure 4b), which is indicative of the covalent bonding between these atoms. Thus, we can argue that there was covalent bonding between the carbon atoms, and the carbon in this structure was in the sp^3-hybridized state.

Table 2. Effective Bader charges on each atom in the relaxed $FeCO_3$-$R\bar{3}c$ and Fe_2CO_4-$P\bar{1}$ at 50 GPa.

$FeCO_3$		Fe_2CO_4	
Atom	**Bader Charge (*e*)**	**Atom**	**Bader Charge (*e*)**
Fe	+1.195	Fe1	+1.282
		Fe2	+1.215
C	+2.228	C	+1.609
O	−1.141	O1	−1.045
		O2	−1.078
		O3	−0.924
		O4	−1.059

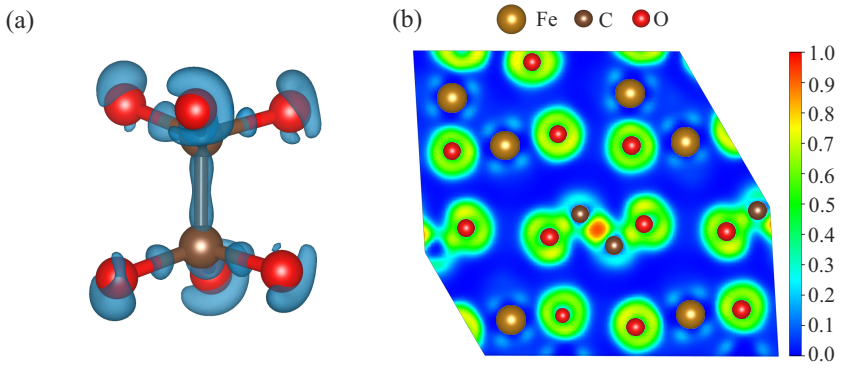

Figure 4. (**a**) Charge density difference and (**b**) electron localization functions of Fe_2CO_4-$P\bar{1}$ at 50 GPa.

To investigate the thermal stability of the predicted Fe_2CO_4-$P\bar{1}$ structure, we performed AIMD calculations at 50 GPa and different temperatures. Although small shifts and Fe^{2+} cation displacements were observed during the entire 10 ps AIMD simulations at temperatures of 300 and 1000 K, the covalent C–C and C–O bonds were not broken, and the Fe atoms were roughly in the same position. At 1000 K, the C–C and C–O distances varied from 1.35 to 1.74 Å and from 1.17 to 1.63 Å, respectively, confirming that there was no breaking of these bonds. At 2000 K, there was also no observed breaking of the C–C and C–O bonds. The C–C and C–O distances varied from 1.29 to 1.81 Å and from 1.11 to 1.72 Å through MD simulation. From Figure 5, it can clearly be seen that at 2000 K, the structure changed. Specifically, some Fe atoms migrated from one octahedral slab to another. Interestingly, with a more thorough analysis of the MD simulation performed at 2000 K, we can conclude that the process of migration of Fe atoms was continuous (Video S1). A similar self-diffusion of iron atoms was observed for the structure of *bcc* iron at pressures of the Earth's inner core and high temperatures [37]. However, nothing similar was observed earlier for carbonate compounds, and only continuous rotation of [CO_3] groups (the so-called dynamical disorder) was described for alkaline earth carbonates [38].

In addition, the thermal stability of the second low-enthalpy phase Fe_2CO_4-$P1$ was investigated. According to the results, it was also stable at 300 and 1000 K, and at 2000 K, a continuous migration of Fe^{2+} cations was observed (Figure S3), but compared with Fe_2CO_4-$P\bar{1}$, it was more intense (Video S2).

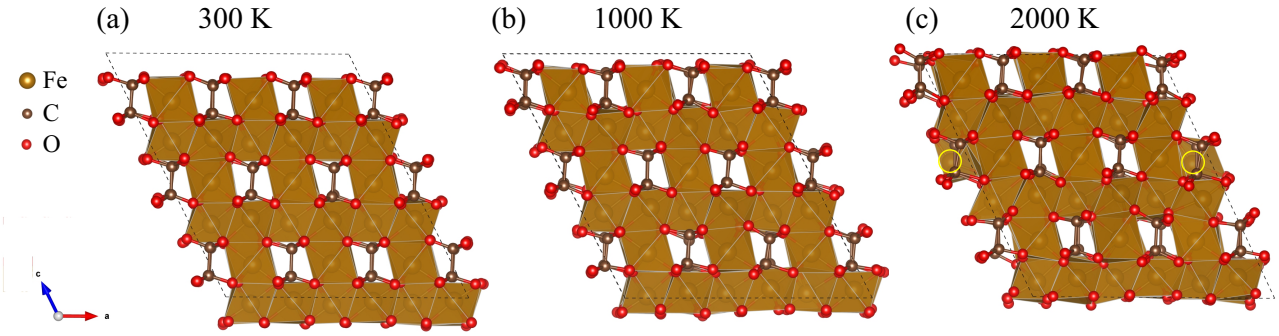

Figure 5. Snapshots of Fe_2CO_4 at the end of the AIMD simulations at 50 GPa and (**a**) 300, (**b**) 1000, and (**c**) 2000 K. The migrated atoms are highlighted in yellow. The dashed line represents the simulated cell.

In traditional carbonates, the cation can be replaced, and numerous alkaline earth and transition metal carbonates can be formed in the same calcite structure, among which are $FeCO_3$, $MnCO_3$, $CoCO_3$, $NiCO_3$, and $ZnCO_3$. Based on this, we performed preliminary calculations to examine the dynamic stability of Mn_2CO_4, Co_2CO_4, Ni_2CO_4, and Zn_2CO_4 in the $P\bar{1}$ structure. No imaginary modes in the phonon spectra of Mn_2CO_4-$P\bar{1}$, Co_2CO_4-$P\bar{1}$, and Ni_2CO_4-$P\bar{1}$ were observed, and hence these orthocarbonates were dynamically

stable (Figure 6). The relaxation of Zn_2CO_4-$P\bar{1}$ was accompanied by the rearrangement of atoms with the destruction of the C–C bonds (i.e., it was not stable against small atomic displacements). Only isolated CO_3 triangles were observed in the final structure of Zn_2CO_4.

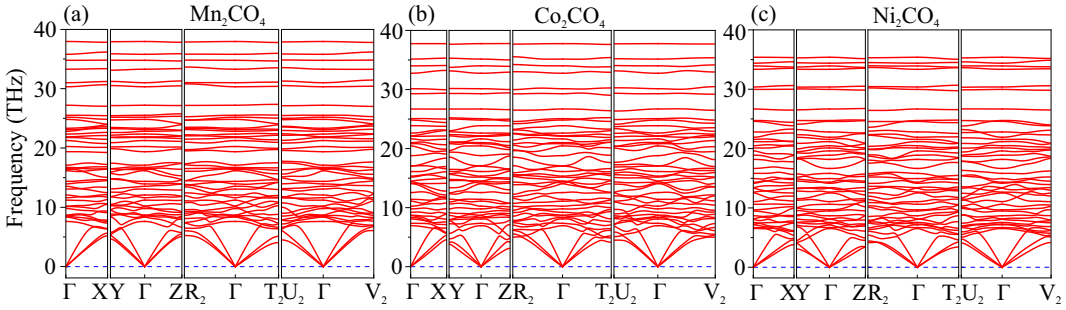

Figure 6. Phonon dispersion curves of (**a**) Mn_2CO_4, (**b**) Co_2CO_4, and (**c**) Ni_2CO_4 in $P\bar{1}$ structure at 50 GPa.

Stable structures of $CaCO_3$ with $[CO_4]$ tetrahedra are known to appear at pressures above 75 GPa [16,39], while Ca_2CO_4 with $[CO_4]$ tetrahedra become stable starting from a pressure of 15 GPa [2,7]. Based on this tendency, according to which the sp^3 structure in the M_2CO_4 composition appears at much lower pressures than in the MCO_3 composition, we assumed that there was a stable structure of $FeCO_3$ with O_3C–CO_3 orthooxalate groups at a pressure several times higher than that for Fe_2CO_4. To examine this assumption, we performed crystal structure prediction calculations at pressures of 100–300 GPa. At 100 and 200 GPa, the siderite structure ($FeCO_3$-$R\bar{3}c$) was predicted to be the most favorable one. At 300 GPa, the new structure of $FeCO_3$ with the symmetry $P\bar{1}$ was predicted to be the most favorable one. As expected, the new $FeCO_3$-$P\bar{1}$ was characterized by the presence of orthooxalate groups. According to our calculations, the phase transition from $FeCO_3$-$R\bar{3}c$ to this structure occurred at a pressure of 275 GPa (Figure 7a). From the calculated phonon spectra, it is clear that $FeCO_3$-$P\bar{1}$ is dynamically stable (Figure 7b). It should be noted that the previously known structures $MgCO_3$-$C2/m$, -$P\bar{1}$, -$P2_1$, and -$Pna2_1$ [15] with $[CO_4]$ tetraherda were also considered in the calculations. However, they were energetically unfavorable in the entire considered pressure range.

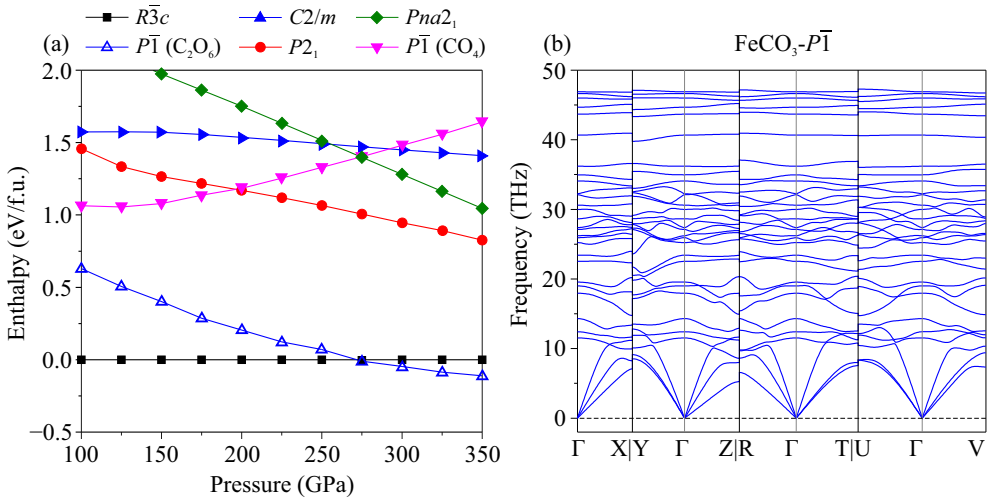

Figure 7. (**a**) Relative enthalpy-pressure dependencies of $FeCO_3$ modifications. (**b**) Phonon dispersion curves of $FeCO_3$-$P\bar{1}$ with $[C_2O_6]$ groups at 300 GPa.

The structural data of the new phase $FeCO_3$-$P\bar{1}$ are given in Table 1. Similar to Fe_2CO_4-$P\bar{1}$, it can be described as an *hcp* array of oxygen atoms in which half of the octahedral voids were filled: 1/3 was filled with Fe atoms, and 1/6 was filled with C–C groups. The A, A',

A", and B octahedral slabs can be distinguished (Figure 8a). In slab A, all octahedral voids were filled with Fe and C–C groups, as shown in Figure 8b, while in slab B, all octahedra were empty. Layers A′ and A" were filled in the same way as layer A but shifted relative to each other by one octahedron.

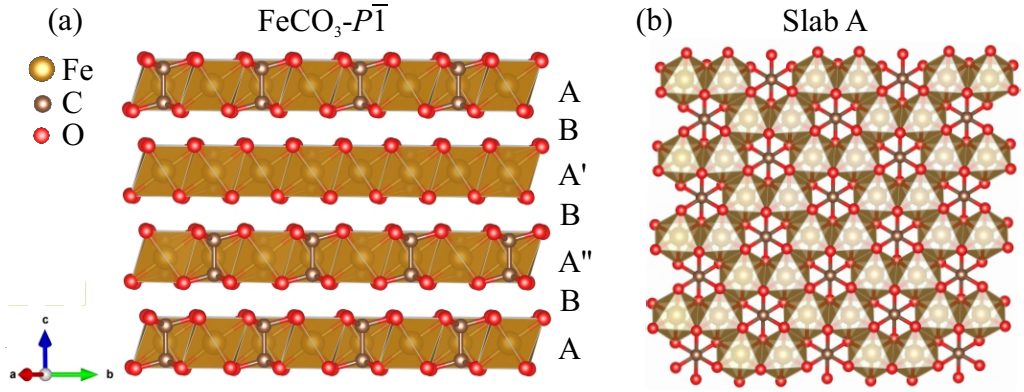

Figure 8. Crystal structure of predicted $FeCO_3$-$P\bar{1}$.

4. Discussion

The formation of $O_3C–CO_3$ orthooxalate groups in melts and aqueous carbonate solutions was proposed earlier by AIMD simulations [40,41]. Solomatova et al. [40] reported that in pyrolite melts ($NaCa_2Fe_4Mg_{30}Al_3Si_{24}O_{89}$) with 6.48 and 9.82 wt% of CO_2 at a pressure of 65 GPa, in addition to [CO_2], [CO_3], and [CO_4], other species with polymerized carbon were also formed. Among the polymerized carbon species, the most observed one was ethane-like [C_2O_6] (i.e., $O_3C–CO_3$ groups). With increasing pressure, the relative number of $O_3C–CO_3$ groups in the melts increases. This could mean that with increasing pressure, $O_3C–CO_3$ groups become more favorable over other polymerized (C_xO_y) species. Kuang and Tse [41] investigated the reactions of hydrogen and calcium carbonate melts at high pressures. It was shown that a calcium carbonate melt contains only [CO_3] and [CO_4] species, while after reaction with H_2, the formation of complex oxo-carbon polymers ([C_xO_y]) displaying C–C bonds, including $O_3C–CO_3$ groups, can be observed. Our results demonstrate the first example of possible solid structures with the same $O_3C–CO_3$ groups.

For Fe_2CO_4, several phases with a similar structure were predicted, which differed only in the distribution of Fe and C–C atoms in the oxygen octahedrons. It is possible that, in reality, Fe_2CO_4 has a structure in which the iron and C–C atoms are statistically distributed through the octahedral voids, especially at high temperatures.

Due to the fact that both $FeCO_3$ ($1FeO*1CO_2$) and Fe_2CO_4 ($2FeO*1CO_2$) presented different filling of octahedral voids in the *hcp* array of oxygen atoms, it can be assumed that the enthalpies of the other structure of intermediate compositions ($xFeO*yCO_2$) will be close to the energetic convex hull, and some of them will be thermodynamically stable.

Supplementary Materials: The following supporting information can be downloaded at https://www.mdpi.com/article/10.3390/sym15020421/s1. Figure S1: Orthooxalate group with C–O and C–C bond distances. Figure S2: Crystal structure of predicted Fe_2CO_4-$P1$. Figure S3: Relaxed structure and snapshots of Fe_2CO_4-$P1$ at the end of the AIMD simulations at 50 GPa and 300, 1000, and 2000 K. Table S1: Structural data of predicted metastable Fe_2CO_4-$P1$. Video S1: AIMD simulation of Fe_2CO_4-$P\bar{1}$ at 50 GPa and 2000 K. Video S2: AIMD simulation of metastable Fe_2CO_4-$P1$ at 50 GPa and 2000 K.

Author Contributions: Conceptualization, P.N.G. and K.D.L.; methodology, N.E.S. and D.N.S.; validation, N.E.S. and P.N.G.; formal analysis, N.E.S. and D.N.S.; investigation, N.E.S. and D.N.S.; writing—original draft preparation, N.E.S., P.N.G., and D.N.S.; writing—review and editing, K.D.L.; visualization, N.E.S. and D.N.S.; supervision, P.N.G. and K.D.L.; funding acquisition, P.N.G. All authors have read and agreed to the published version of the manuscript.

Funding: This research was funded by the RFBR under research project no. 20-03-00774 and the state assignment of the IGM SB RAS.

Data Availability Statement: Not applicable.

Acknowledgments: The computations were performed using resources provided by the Novosibirsk State University Supercomputer Center.

Conflicts of Interest: The authors declare no conflict of interest.

References

1. Yao, X.; Xie, C.; Dong, X.; Oganov, A.R.; Zeng, Q. Novel high-pressure calcium carbonates. *Phys. Rev. B* **2018**, *98*, 014108. [CrossRef]
2. Sagatova, D.; Shatskiy, A.; Sagatov, N.; Gavryushkin, P.N.; Litasov, K.D. Calcium orthocarbonate, Ca_2CO_4-*Pnma*: A potential host for subducting carbon in the transition zone and lower mantle. *Lithos* **2020**, *370*, 105637. [CrossRef]
3. Gavryushkin, P.N.; Sagatova, D.N.; Sagatov, N.; Litasov, K.D. Formation of Mg-Orthocarbonate through the Reaction $MgCO_3$+ MgO= Mg_2CO_4 at Earth's Lower Mantle P–T Conditions. *Cryst. Growth Des.* **2021**, *21*, 2986–2992. [CrossRef]
4. Gavryushkin, P.N.; Sagatova, D.N.; Sagatov, N.; Litasov, K.D. Orthocarbonates of Ca, Sr, and Ba—The Appearance of sp^3-Hybridized Carbon at a Low Pressure of 5 GPa and Dynamic Stability at Ambient Pressure. *ACS Earth Space Chem.* **2021**, *5*, 1948–1957. [CrossRef]
5. Banaev, M.V.; Sagatov, N.E.; Sagatova, D.N.; Gavryushkin, P.N. High-Pressure Crystal Structures of Pb_2CO_4 and PbC_2O_5 with Tetrahedral [CO_4] and Pyrocarbonate [C_2O_5] atomic groups. *ChemistrySelect* **2022**, *7*, e202201940. [CrossRef]
6. Gavryushkin, P.; Martirosyan, N.; Rashchenko, S.; Sagatova, D.; Sagatov, N.; Semerikova, A.; Fedotenko, T.; Litasov, K. First Experimental Synthesis of Mg Orthocarbonate by the $MgCO_3$ + MgO= Mg_2CO_4 Reaction at Pressures of the Earth's Lower Mantle. *JETP Lett.* **2022**, *116*, 477–484. [CrossRef]
7. Binck, J.; Laniel, D.; Bayarjargal, L.; Khandarkhaeva, S.; Fedotenko, T.; Aslandukov, A.; Glazyrin, K.; Milman, V.; Chariton, S.; Prakapenka, V.B.; et al. Synthesis of calcium orthocarbonate, Ca_2CO_4-Pnma at P-T conditions of Earth's transition zone and lower mantle. *Am. Mineral.* **2022**, *107*, 336–342. [CrossRef]
8. König, J.; Spahr, D.; Bayarjargal, L.; Gavryushkin, P.N.; Sagatova, D.; Sagatov, N.; Milman, V.; Liermann, H.P.; Winkler, B. Novel Calcium sp^3 Carbonate CaC_2O_5-$I4\bar{2}d$ May Be a Carbon Host in Earth's Lower Mantle. *ACS Earth Space Chem.* **2022**, *6*, 73–80. [CrossRef]
9. Laniel, D.; Binck, J.; Winkler, B.; Vogel, S.; Fedotenko, T.; Chariton, S.; Prakapenka, V.; Milman, V.; Schnick, W.; Dubrovinsky, L.; et al. Synthesis, crystal structure and structure–property relations of strontium orthocarbonate, Sr_2CO_4. *Acta Crystallogr. Sect. B* **2021**, *77*, 131–137. [CrossRef]
10. Spahr, D.; König, J.; Bayarjargal, L.; Gavryushkin, P.N.; Milman, V.; Liermann, H.P.; Winkler, B. $Sr_3[CO_4]O$ Antiperovskite with Tetrahedrally Coordinated sp^3-Hybridized Carbon and OSr_6 Octahedra. *Inorg. Chem.* **2021**, *60*, 14504–14508. [CrossRef]
11. Spahr, D.; König, J.; Bayarjargal, L.; Milman, V.; Perlov, A.; Liermann, H.P.; Winkler, B. $Sr[C_2O_5]$ is an Inorganic Pyrocarbonate Salt with $[C_2O_5]^{2-}$ Complex Anions. *J. Am. Chem. Soc.* **2022**, *144*, 2899–2904. [CrossRef] [PubMed]
12. Spahr, D.; König, J.; Bayarjargal, L.; Luchitskaia, R.; Milman, V.; Perlov, A.; Liermann, H.P.; Winkler, B. Synthesis and Structure of $Pb[C_2O_5]$: An Inorganic Pyrocarbonate Salt. *Inorg. Chem.* **2022**, *61*, 9855–9859. [CrossRef] [PubMed]
13. Sagatova, D.N.; Gavryushkin, P.N.; Sagatov, N.E.; Banaev, M.V. High-pressure transformations of CaC_2O_5—A full structural trend from double [CO_3] triangles through the isolated group of [CO_4] tetrahedra to framework and layered structures. *Phys. Chem. Chem. Phys.* **2022**, *24*, 23578–23586. [CrossRef] [PubMed]
14. Oganov, A.R.; Glass, C.W.; Ono, S. High-pressure phases of $CaCO_3$: Crystal structure prediction and experiment. *Earth Planet. Sci. Lett.* **2006**, *241*, 95–103. [CrossRef]
15. Pickard, C.J.; Needs, R.J. Structures and stability of calcium and magnesium carbonates at mantle pressures. *Phys. Rev. B* **2015**, *91*, 104101. [CrossRef]
16. Smith, D.; Lawler, K.V.; Martinez-Canales, M.; Daykin, A.W.; Fussell, Z.; Smith, G.A.; Childs, C.; Smith, J.S.; Pickard, C.J.; Salamat, A. Postaragonite phases of $CaCO_3$ at lower mantle pressures. *Phys. Rev. Mater.* **2018**, *2*, 013605. [CrossRef]
17. Binck, J.; Bayarjargal, L.; Lobanov, S.S.; Morgenroth, W.; Luchitskaia, R.; Pickard, C.J.; Milman, V.; Refson, K.; Jochym, D.B.; Byrne, P.; et al. Phase stabilities of $MgCO_3$ and $MgCO_3$-II studied by Raman spectroscopy, x-ray diffraction, and density functional theory calculations. *Phys. Rev. Mater.* **2020**, *4*, 055001. [CrossRef]
18. Cerantola, V.; Bykova, E.; Kupenko, I.; Merlini, M.; Ismailova, L.; McCammon, C.; Bykov, M.; Chumakov, A.I.; Petitgirard, S.; Kantor, I.; et al. Stability of iron-bearing carbonates in the deep Earth's interior. *Nat. Commun.* **2017**, *8*, 1–9. [CrossRef]
19. Nagai, T.; Ishido, T.; Seto, Y.; Nishio-Hamane, D.; Sata, N.; Fujino, K. Pressure-induced spin transition in $FeCO_3$-siderite studied by X-ray diffraction measurements. *J. Phys. Conf. Ser.* **2010**, *215*, 012002. [CrossRef]
20. Zhao, C.; Xu, L.; Gui, W.; Liu, J. Phase Stability and Vibrational Properties of Iron-Bearing Carbonates at High Pressure. *Minerals* **2020**, *10*, 1142. [CrossRef]
21. Oganov, A.R.; Glass, C.W. Crystal structure prediction using ab initio evolutionary techniques: Principles and applications. *J. Chem. Phys.* **2006**, *124*, 244704. [CrossRef] [PubMed]

22. Oganov, A.R.; Lyakhov, A.O.; Valle, M. How Evolutionary Crystal Structure Prediction Works–and Why. *Accounts Chem. Res.* **2011**, *44*, 227–237. [CrossRef] [PubMed]
23. Lyakhov, A.O.; Oganov, A.R.; Stokes, H.T.; Zhu, Q. New developments in evolutionary structure prediction algorithm USPEX. *Comput. Phys. Commun.* **2013**, *184*, 1172–1182. [CrossRef]
24. Bushlanov, P.V.; Blatov, V.A.; Oganov, A.R. Topology-based crystal structure generator. *Comput. Phys. Commun.* **2019**, *236*, 1–7. [CrossRef]
25. Pickard, C.J.; Needs, R.J. High-Pressure Phases of Silane. *Phys. Rev. Lett.* **2006**, *97*, 045504. . 97.045504. [CrossRef] [PubMed]
26. Pickard, C.J.; Needs, R.J. Ab initio random structure searching. *J. Phys. Condens. Matter* **2011**, *23*, 053201. . 88/0953-8984/23/5/053201. [CrossRef]
27. Kresse, G.; Furthmüller, J. Efficient iterative schemes for ab initio total-energy calculations using a plane-wave basis set. *Phys. Rev. B* **1996**, *54*, 11169–11186. [CrossRef]
28. Kresse, G.; Furthmüller, J. Efficiency of ab-initio total energy calculations for metals and semiconductors using a plane-wave basis set. *Comput. Mater. Sci.* **1996**, *6*, 15–50. [CrossRef]
29. Perdew, J.P.; Burke, K.; Ernzerhof, M. Generalized gradient approximation made simple. *Phys. Rev. Lett.* **1996**, *77*, 3865. [CrossRef]
30. Dudarev, S.L.; Botton, G.A.; Savrasov, S.Y.; Humphreys, C.J.; Sutton, A.P. Electron-energy-loss spectra and the structural stability of nickel oxide: An LSDA+U study. *Phys. Rev. B* **1998**, *57*, 1505–1509. [CrossRef]
31. Li, Z.; Stackhouse, S. Iron-rich carbonates stabilized by magnetic entropy at lower mantle conditions. *Earth Planet. Sci. Lett.* **2020**, *531*, 115959. [CrossRef]
32. Togo, A.; Tanaka, I. First principles phonon calculations in materials science. *Scr. Mater.* **2015**, *108*, 1–5. [CrossRef]
33. Momma, K.; Izumi, F. VESTA: A three-dimensional visualization system for electronic and structural analysis. *J. Appl. Crystallogr.* **2008**, *41*, 653–658. [CrossRef]
34. Stukowski, A. Visualization and analysis of atomistic simulation data with OVITO–the Open Visualization Tool. *Model. Simul. Mater. Sci. Eng.* **2009**, *18*, 015012. [CrossRef]
35. Aped, P.; Fuchs, B.; Goldberg, I.; Senderowitz, H.; Tartakovsky, E.; Weinman, S. Structure and conformation of heterocycles. 21. Probing the anomeric effect in orthoesters. Structure, conformation, and dynamic behavior of a unique orthooxalate: 2, 5, 7, 10, 11, 14-hexaoxa [4.4. 4] propellane. *J. Am. Chem. Soc.* **1992**, *114*, 5585–5590. [CrossRef]
36. Junk*, P.C. Supramolecular interactions in the X-ray crystal structure of potassium tris (oxalato) ferrate (III) trihydrate. *J. Coord. Chem.* **2005**, *58*, 355–361. [CrossRef]
37. Belonoshko, A.B.; Lukinov, T.; Fu, J.; Zhao, J.; Davis, S.; Simak, S.I. Stabilization of body-centred cubic iron under inner-core conditions. *Nat. Geosci.* **2017**, *10*, 312–316. [CrossRef]
38. Ishizawa, N. Calcite V: A hundred-year-old mystery has been solved. *Powder Diffr.* **2014**, *29*, S19–S23. [CrossRef]
39. Gavryushkin, P.N.; Martirosyan, N.S.; Inerbaev, T.M.; Popov, Z.I.; Rashchenko, S.V.; Likhacheva, A.Y.; Lobanov, S.S.; Goncharov, A.F.; Prakapenka, V.B.; Litasov, K.D. Aragonite-II and $CaCO_3$-VII: New High-Pressure, High-Temperature Polymorphs of $CaCO_3$. *Cryst. Growth Des.* **2017**, *17*, 6291–6296. [CrossRef]
40. Solomatova, N.V.; Caracas, R.; Manning, C.E. Carbon sequestration during core formation implied by complex carbon polymerization. *Nat. Commun.* **2019**, *10*, 789. [CrossRef]
41. Kuang, H.; Tse, J.S. High-Temperature, High-Pressure Reactions of H_2 with $CaCO_3$ Melts. *Phys. Status Solidi B* **2022**, *259*, 2100644. [CrossRef]